Advances in Computational Design, *Vol. 7, No. 4 (2022) 371-393*
https://doi.org/10.12989/acd.2022.7.4.371

Three-dimensional analysis of flexible pavement in Nepal under moving vehicular load

Bijay Ban[a], Jagat K. Shrestha[b], Rojee Pradhananga[c] and Kshitij C. Shrestha[1*]

Department of Civil Engineering, Pulchowk Campus, Institute of Engineering, Tribhuvan University, Lalitpur, Nepal

(Received November 15, 2021, Revised August 17, 2022, Accepted August 18, 2022)

Abstract. This paper presents a three-dimensional flexible pavement simulated in ANSYS subjected to moving vehicular load on the surface of the pavement typical for the road section in Nepal. The adopted finite element (FE) model of pavement is validated with the classical theoretical formulations for half-space pavement. The validated model is further utilized to understand the damping and dynamic response of the pavement. Transient analysis of the developed FE model is done to understand the time varying response of the pavement under a moving vehicle. The material properties of pavement considered in the analysis is taken from typical road section used in Nepal. The response quantities of pavement with nonlinear viscoelastic asphalt layer are found significantly higher compared to the elastic pavement counterpart. The structural responses of the pavement decrease with increase in the vehicle speed due to less contact time between the tires of the vehicle and the road pavement.

Keywords: flexible pavement, moving vehicular load; three-dimensional analysis; transient analysis; viscoelastic material

1. Introduction

The overall functioning of the highway system greatly relies on the performance of its pavements. Pavement distress, life cycle, and overall functioning are determined by the pavements' design procedure. Empirical methods, namely, American Association of State Highway Transportation Officials (AASHTO, 1993) and Road Note-31 by Transport and Road Research Laboratory (TRRL) UK (Road Note 31, 1984) are followed for the design of the flexible pavements worldwide. Department of Roads (DOR), Nepal has provided a guideline for the design of flexible pavements (DOR, 2021) which uses both empirical and mechanistic-empirical method following the Indian Road Congress IRC 37 -2018 (IRC 2018) guideline, American Association of State Highway and Transportation Officials (AASHTO 1993) Guides for Design of Pavement Structures, and Road Note-31 (1984). The guidelines of DOR suggests design of flexible pavements using IITPAVE software (IRC, 2018) which considers pavement as a multi-layered

*Corresponding author, Ph.D., E-mail: kshitij.shrestha@pcampus.edu.np
[a]M.Sc. Student, E-mail: bijay_ban@outlook.com
[b]Ph.D., E-mail: jagatshrestha@ioe.edu.np
[c]Ph.D., E-mail: rojee.pradhananga@pcampus.edu.np

Copyright © 2022 Techno-Press, Ltd.
http://www.techno-press.org/?journal=acd&subpage=7 ISSN: 2383-8477 (Print), 2466-0523 (Online)

structure and stresses and strains at critical locations are computed using the linear elastic model (DOR 2021). Mechanistic-empirical approaches can provide better insight for designing with the various combinations of material properties and its stress and strain nature in the pavement layers. Application and use of new computational techniques and finite elements (FE) have contributed to strong improvements in pavement simulation and analysis.

Several approaches have been adopted to model pavement using finite element (FE) model. Lu and Wright (1998) in their research paper simulated pavement using a two-dimensional 2D plane strain model. Li *et al*. (2017) simulated using 2D FE axisymmetric model to evaluate pavement performance. However, the three-dimensional simulations gave more reasonable results than the two-dimensional simulations, when compared with actual measurements under traffic loading. Cho *et al*. (1996), Zaghloul *et al*. (1994) were among some of the first to develop a 3-D model which is capable to capture the response of moving load. Later, several 3-D finite element models have been purposed by various researchers (Beskou *et al*. 2016a, b, Gungor *et al*. 2016, Huang *et al*. 2001, Yoo and Al-Qadi 2007, Melaku and Qiu 2015, Byzyka *et al*. 2020).

Accurate modeling analysis of the pavement system also requires adopting an ideal constitutive model for each layer of pavement in simulation (Ali *et al*. 2009, Li *et al*. 2017). The use of elastic material properties underestimates pavement response by a lot compared to that of actual response (Beskou *et al*. 2016a). Thus, the need of nonlinear material properties modeling has arisen. Researchers have been using nonlinear material properties of pavement to simulate the response of FEM closer to actual response under vehicular loading. Among the notable previous works, Beskou *et al*. (2016a, b); Cebon (1999); González *et al*. (2007); Huang *et al*. (2011); Li *et al*. (2017); Saleeb *et al*. (2005) have used viscoelastic and viscoplastic constitutive models in FE simulation.

Further, modeling of vehicular loading and its simulation techniques is also important to simulate the response of pavement structure. The load exerted by vehicles on the pavement is non-uniform and depends on the tire construction, tire load, and tire inflation pressure (De Beer 1996), resulting in complexity in modeling. So, for the simulation of vehicular loading, various loading simulations are considered according to their accuracy and convenience. Vehicular loading has been simulated as pulse rolling load (Lu and Wright 1998), stationary transient loading (Howard and Warren 2009), impulse loading (Ali *et al*. 2009, Cebon 1999), dynamic loading by moving coordinate (Shen and Kirkner 2001) and transient local dynamic loading (Assogba *et al*. 2020, Yoo and Al-Qadi 2007). The use of dynamic loading in the FE simulation results in a much closer response of nature under vehicular loading than static FE simulation using nonlinear properties (Beskou *et al*. 2016, Huang *et al*. 2001).

In this study, a three-dimensional FE model of pavement is simulated in the ANSYS Mechanical Ansys Parametric Design Language (APDL) (DeSalva and Swanson 1985b, ANSYS 2013) in the working platform of commercial software ANSYS 2020 R2. The validated FE model is further subjected to various loading parameter to understand the response of the pavement. Both elastic and non-linear material characteristics are studied in this work. The developed FE model is capable of simulating the response of a flexible pavement subjected to vehicular loading. The model is applied for various pavements' composition/thickness under the loading to get insight into the effect of its structural response. A thorough discussion is made to understand the effect of vehicular motion with different velocities on stresses and strains experienced by the pavement particularly for Nepalese conditions, which has not been documented yet. The work will help to approach the pavement designs in Nepalese context through a detailed computational technique and FE based design considering both linear and non-linear material characteristics.

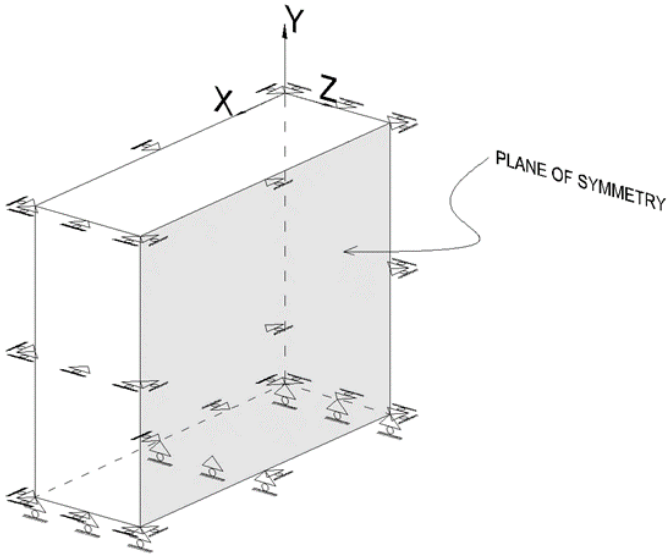

Fig. 1 Boundary conditions for finite element modeling of pavement

2. Finite element model generation

A 3D FE model is prepared in ANSYS (DeSalva and Swanson 1985a, ANSYS 2013) using 8-noded structural solid brick element). The 2x2x2 integration point is taken for the calculation of stiffness, stress and mass matrices while the 2x2 integration point is taken for the pressure load vector.

2.1 Boundary condition

The boundary condition applied to the pavement structure play important role in the result of the analysis. As pavement is continuous structure in nature, modeling of the pavement with any boundary condition results in some error in analysis. Assogba *et al*. (2020) and Li *et al*. (2017) have used continuum element in boundaries to replicate the continuum domain in analysis, also absorbing boundaries have been used to minimize the boundary effect on the pavement responses (Hatzigeorgiou and Beskos, 2010). The analysis from Beskou *et al*. (2016b) has shown that if a sufficiently large dimension of a model with the rollers, the boundary doesn't have a significant effect on the value of the responses of pavement as the reaction from boundary gets diminished coming to point of interest in the model. Having large geometry does provide a more accurate result as boundaries effect on it is minimized but it does require high computational times. The dimension of the model is determined after conducting various trials and errors to get a balance between accuracy and computational time. The vertical dimension has a significant effect on the accuracy of result, thus, a large vertical dimension over other dimension is considered in the analysis as done by Assogba *et al*. (2020) and Beskou *et al*. (2016b).

Further, the model with roller boundaries provides a similar result with the model having absorbing boundaries (Beskou *et al*. 2016b). This study also utilizes simple roller boundaries in pavement modeling as illustrated in Fig. 1. The vertical displacement decreases as depth increases,

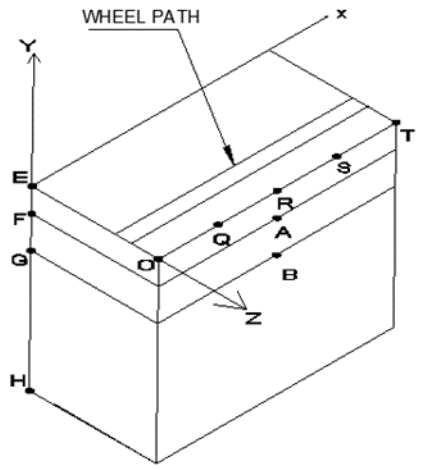

Fig. 2 A typical section of flexible pavement with pavement layers of asphalt-EF, base-FG and subgrade-GH. Vehicle load moves from Point Q to S along the wheel path

and it is assumed that the vertical displacement at the bottom of the pavement is negligible, therefore, the bottom of the pavement in FE model is constrained in vertical direction. The pavement in nature is restrained in the lateral direction by its surrounding soil, so in the FE model, the lateral movement of pavement is also assumed to be constrained by applying roller on its lateral sides. The vehicle loading and pavement considered in this is symmetrical about the x-y axis, thus, only half of pavement and loading is considered during simulation. The roller boundary is applied on axis of symmetricity and the pavement is restrained sufficiently to prevent the rigid body movement under loading.

2.2 Element type, size and meshing

Fig. 2 shows the 3D FE model of the flexible pavement with dimensions of 25.8m x 11.5m x 35m. The pavement generally consists of four layers, asphalt, base, subbase and subgrade. The elastic material properties of base and subbase are nearly similar so only three layers are considered for current FE modeling of the pavement as shown in Fig. 2 with asphalt layer represented as EF, base layer as FG and subgrade as GH. Vehicle load moves from Point Q to S along the wheel path. Fig. 3 shows the generated FE model mesh. The model is meshed with relatively finer mesh of element size of 0.115 m near the loading region and the area where high stress is developed. A relatively coarse mesh of average element size of 0.5 m with their own bias in spacing along its layers is adopted elsewhere. A total of 2,80,342 eight-noded solid brick elements are generated for the development of the FE model.

2.3 Material characterization

Mechanistic empirical-based pavement design methodology requires mathematical modeling of the material behavior of pavement layers. The material behavior of any material is extremely

Table 1 Pavement elastic material properties

Layers	Thickness (m)	Young Modulus, E (MPa)	Poisson Ratio, μ	Density (kg/m^3)
Asphalt	0.19	2000	0.35	2500
Base	0.47	200	0.35	2667
Subgrade	34.33	62	0.35	1990

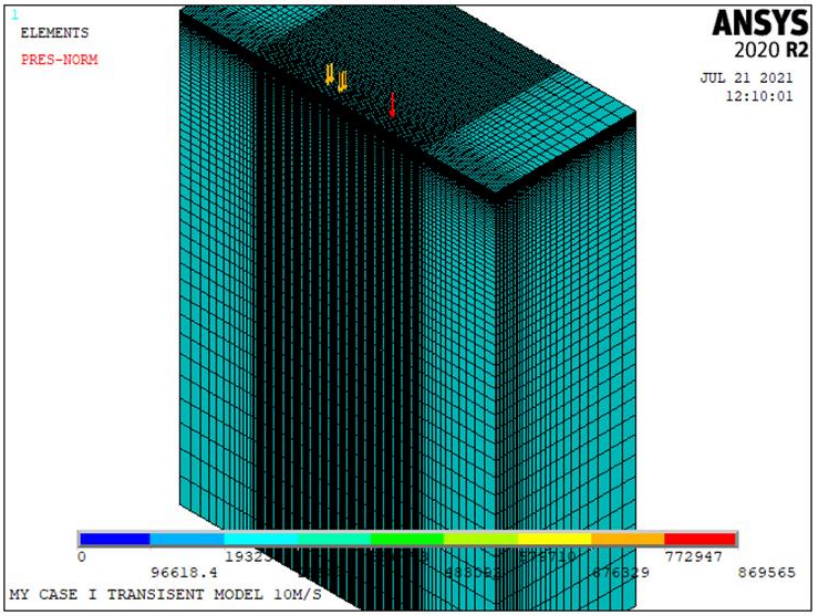

Fig. 3 Three-dimensional finite element model of flexible pavement

complex. The material behavior of pavement layers is approximated by various mathematical models depending on the purpose and the required precision of the model predictions. The elastic model can be used to represent engineering material provided that the strains (ε) are significantly small. Further, upon unloading the body returns to its original position and doesn't depend on the rate of loading.

The nonlinear model is generally used to represent the more accurate material response and the response of the material is a complex function of strain, rate of strain, strain history, etc. The model using linear elastic constitutive relation results in simplification in the modeling and computation. However, the result from linear constitutive modeling helps in the intuitive understanding of the response of the structure and provide valuable insight for nonlinear modeling. For the preliminary understanding of the pavement response during the vehicle loading, a linear mathematical model is used before going to a nonlinear mathematical model. The present work is based on linear as well as nonlinear constitutive models of the pavement material.

The elastic material properties of the pavement layers are shown in Table 1 taken of commonly used value for road design in the Kathmandu valley as per DOR guidelines (DOR 2014). No interface element was modeled between layers of the pavement and the layers are assumed to be perfectly bonded.

The work from Beskou *et al*. (2016a) has shown that pavement response with viscoelastic asphalt layer and elastic properties on other layers exhibits similar dynamic behavior and response results to consider nonlinearity on base and subgrade layers. Thus, the nonlinear pavement analysis is carried out by including nonlinearity in the asphalt layer only with the linear properties in other pavement layers. The material behavior of asphalt is both time-dependent and temperature-dependent and was modeled as viscoelastic material whose stiffness depends on time, temperature, and the frequency of the applied load (Li *et al*. 2015, Gungor *et al*. 2016). The hereditary integral formulation of the generalized Maxwell model was used to express asphalt viscoelasticity. Material data of retardation time (τ_i) and shear relaxation modulus (G_i) are required to define viscoelasticity for which four prony term was used.

The nonlinear material characteristics of asphalt was modeled as viscoelastic whose stiffness depends on time, temperature, and the frequency of the applied load (Gungor *et al*. 2016, Li *et al*. 2016). A generalized Maxwell model was used to model the viscoelastic behavior of asphalt layer and to simulate the dynamic behavior. The hereditary integral formulation of an isotropic viscoelastic material stress function can be expressed as Eq. (1) (DeSalva and Swanson 1985a).

$$\sigma(t) = \int_0^t 2G_{(t-\tau)} \frac{de}{dt} d\tau + I \int_0^t K_{(t-\tau)} \frac{d\Delta}{d\tau} d\tau \tag{1}$$

where $\sigma(t)$ is the stress, $G(\underline{t})$ is the shear relaxation kernel function, $K(t)$ is bulk/volume relaxation kernel function, e is the strain deviator (shear deformation), Δ is the bulk deviator (volume deformation), t is reduced relaxation time, I is tensor unit.

Prony-Dirichlet Series was used to represent the time dependency response of the asphalt concrete (DeSalva and Swanson, 1985a). Eqs. (2)-(3) shows the constitutive models for shear modulus and bulk modulus.

$$G_{(t)} = G_\infty + \sum_{i=1}^{n} G_i . \exp(-t/\tau_i) \tag{2}$$

$$K_{(t)} = K_\infty + \sum_{i=1}^{n} K_i . \exp(-t/\tau_i) \tag{3}$$

where $G_i, G_\infty, K_i, K_\infty$ are initial and equilibrium values for $G_{(t)}$ and $K_{(t)}$, τ_i is the retardation time, t is the reduced relaxation time, n is the series number.

The shear and bulk moduli of asphalt concrete were determined from the relaxation modulus $E(t)$ using Eqs. (4)-(5).

$$G(t) = \frac{E(t)}{2(1+\mu)} \tag{4}$$

$$K(t) = \frac{E(t)}{3(1-3\mu)} \tag{5}$$

Table 2 shows material data of retardation time (τ_i) and shear relaxation modulus (G_i) required to define viscoelasticity for which four prony terms were used. The value of material constant (G_i) is taken from the experimental results of Berthelot *et al*. (2003), which is scaled from $G(0) = 817$

Table 2 Prony-Dirichlet Series for generalized Maxwell Model

No.	τ_i(s)	G_i(MPa)
1	20.0	3.92×10^1
2	2.0	1.23×10^2
3	1.0	1.19×10^1
4	0.2	3.04×10^2
∞	-	2.59×10^2

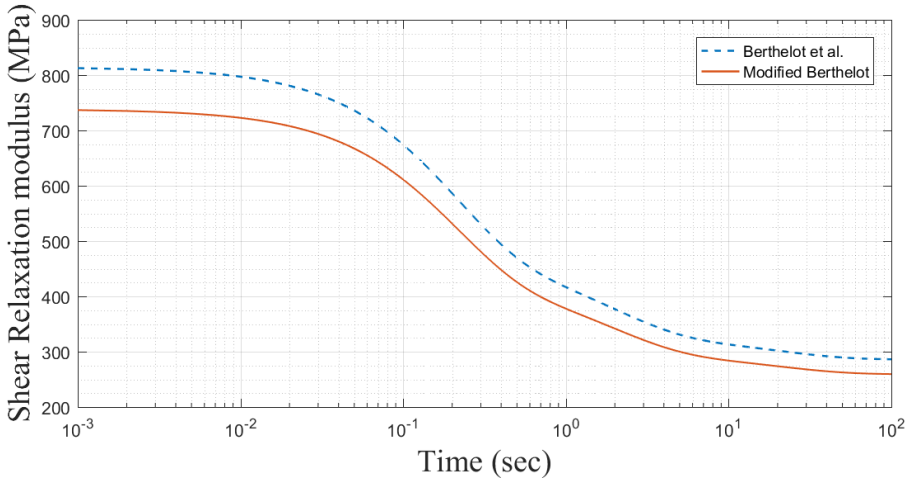

Fig. 4 Shear relaxation modulus of asphalt material

Table 3 Vehicle specification

Vehicle	LPK 2518 6S 20 cum
Wheel Base	4880 mm
Weight (Gross Vehicle Weight)	25000 Kg
Overall Length	8530 mm
Overall Width	2400 mm
Tire	10.00 x 20 – 16 PR
Inflation Pressure	109 psi

MPa (Asphalt Specimen 900901) to $G(0)$ = 740.7 MPa for $E(t)$ of 2000 MPa and μ of 0.35 to be compatible with the elastic properties of the asphalt layer taken for road design in the Kathmandu valley as per DOR guidelines (DOR 2014). The adopted shear relaxation modulus versus time plot is illustrated in Fig. 4. The temperature of pavement is assumed constant at 20ºC.

2.4 Modeling of vehicle and loading strategy

For analysis of response of pavement due to vehicle load, a representative vehicle LPK 2518 6S 20 cum (Tata-Motor 2020) is chosen as a model vehicle in this research. It should be noted that this is a commonly available truck in Nepal. The dimension of the vehicle is shown in Table 3.

Table 4 Details of considered Truck LPK 2518, 6s 20 cum weight and tire contact area

Parameter	First-axle wheel	Tandem-axle wheel
Wheel configuration	Single	Dual
Gross vehicle weight on axle (kN)	60	190
Inflation pressure (Psi)	109	109
Tire pavement contact area (cm^2)	399	316
Length of elliptical footprint L (mm)	276	246
Length of equivalent area, 0.87L (mm)	240	214
Width of equivalent area, 0.6L (mm)	166	147

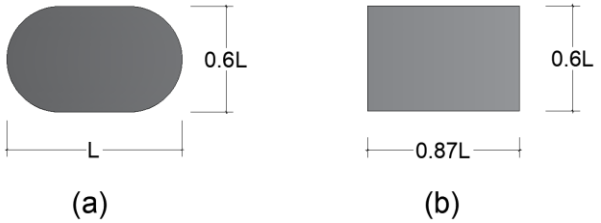

Fig. 5 Tire footprint: (a) Elliptical footprint of tire (b) Equivalent rectangle footprint of tire

The actual representation of moving vehicle loading in a finite element model is complex. The stresses exerted by vehicles on the pavement are non-uniform and depend on the tire construction, tire load, and tire inflation pressure (De Beer 1996). To simulate moving vehicle, the stress distribution is considered to be uniform and rectangular, which results in computational simplification. In reality, the vehicle footprint is elliptical (Y. H. Huang 2004) and contact stress on the pavement is coupled between tires and pavement. The elliptical tire footprint is converted into a rectangle equivalent area (Fig. 5) of length and width 0.87L and 0.6L, respectively, where L is length of elliptical footprint. The load on the wheel axle of a vehicle varies due to non-uniform load distribution on the steering and tandem axle resulting in the tire–pavement contact area varied from the one-wheel tire to another. For numerical modeling purposes and to simplify the APDL code, the tire-pavement contact stress is assumed to be equal to that of inflation pressure of the tire (Table 4), and the tire–pavement contact surface is assumed to be the same between all tires. The equivalent length and the width of each tire footprint are taken as 23 cm and 15 cm respectively.

The vertical contact pressure was only considered to simulate the dynamic effect of the pavement as the horizontal component is assumed not to have a significant impact on the pavement response according to the principle of Saint-Venant (1855). Further, modeling the three-directional tire–pavement contact forces is beyond the scope of this work.

The vehicle configuration as shown in Fig. 6 is taken for the vehicle model. The movement of vehicle is simulated by applying contact stress on area (I) when the wheel of a vehicle is in area (I) at the time t. Next, as wheel moves to the area (I +1) at the time (t+1), the contact stress is applied in area (I+1) and stress is released on area (I). The load is applied as a ramp force between the time interval of loading and unloading forming a triangular variation. The triangular load variation is very close to that of a haversine variation (Huang 2004). The load step is repeated as the vehicle moves on the pavement. Taking symmetricity of the adopted FE model, only half of the loading is applied. The wheel configuration on lateral direction of pavement is shown in Fig. 6.

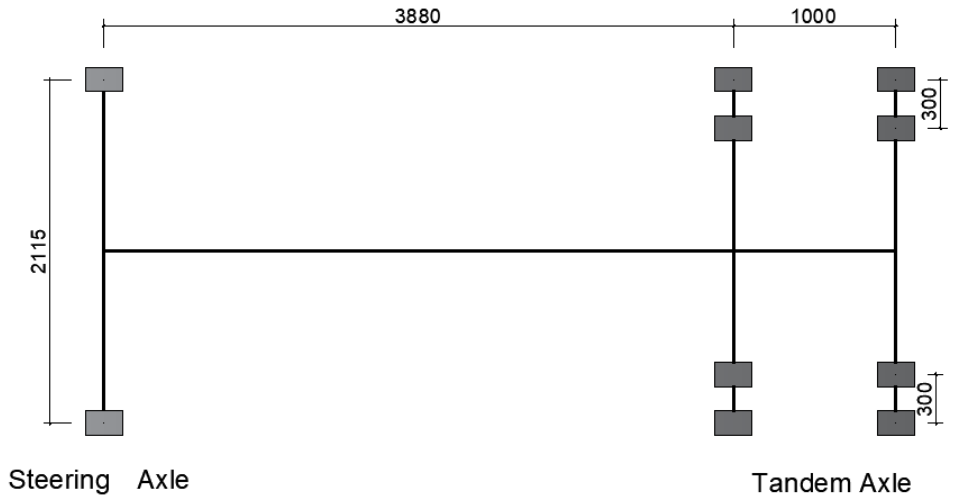

Fig. 6 Finite element modeling of Vehicle LPK 2518c (All dimensions in mm)

2.5 Analysis procedures

The types of analysis to be performed on the structure depend on the nature of loading. In this study, analysis of pavement has been carried out for static and dynamic loading conditions. Static analysis (Eq. (6)) is generally performed when the loading is such that the inertia forces can be neglected in which the acceleration of the body is zero or near about.

$$[K]\{u\} = F \tag{6}$$

For the structure subjected to significantly large accelerated loading, resulting in significant inertia force, the inertial force along with damping is included in the equilibrium Eq. (7) for dynamic analysis.

$$[M]\{\ddot{u}\} + [C]\{\dot{u}\} + [K]\{u\} = F(t) \tag{7}$$

where, [M], [C] and [K] are mass, damping, and stiffness matrix of structure and $\ddot{u}$, $\dot{u}$ and u are acceleration, velocity, and deformation of the structure. External force $F(t)$ represents the vehicle load applying on the surface of the pavement. The vehicle is assumed to be initially in rest position, i.e., $\dot{u}$ and u are zero as an initial condition for the equilibrium Eq. (7).

Equilibrium Eq. (7) is solved in the time domain using the transient analysis option in ANSYS. In transient dynamic analysis, equations are solved considering a set of static equilibrium equations at that given time taking into account inertia forces and damping forces. Newmark's time integration method is used to solve these equations at discrete times. There are two methods available to do transient dynamic analysis, full and mode-superposition methods (DeSalva and Swanson, 1985a). Out of the two methods, full method is chosen. Sparse solver is used to solve the system of simultaneous equation.

Transient analysis of pavement is performed with different velocities to understand the response of the pavement. The response of pavement is determined at two critical locations: a) Point A: asphalt – base interaction (y = 0.19 m), b) Point B: base- subgrade interaction (y = 0.67

m). During the dynamic loading of the pavement, the response of the pavement is oscillatory along the wheel path. Therefore, for the comparison propose, maximum response along the wheel path is considered for each loading case.

3. Results and discussion

3.1 Validation of the FE model

Validation of the model, its meshing, boundary conditions, geometry loading, and the solution is conducted by comparing the result of the developed model in ANSYS to that of theoretical value (Boussinesq 1885). For the elastic half-space, the theoretical value for the vertical displacement and stresses along the x, y, and z-axis of the pavement under the distributed load, p, acting on the circular area of radius α on the surface of the pavement at a depth, z, can be determined by Eqs. (8)-(10) (Boussinesq 1885).

$$u_y = \frac{(1+v)p\alpha}{E} + \left[\left(1+\left(\frac{z}{\alpha}\right)^2\right)^{-0.5} + (1-2v)\left(1+\left(\frac{z}{\alpha}\right)^2\right)^{-0.5} - \left(\frac{z}{\alpha}\right)\right] \tag{8}$$

$$\sigma_y = p\left[1-\left(1+\left(\frac{\alpha}{z}\right)^2\right)^{-1.5}\right] \tag{9}$$

$$\sigma_x = \sigma_z = p\left[\frac{(1+2v)}{2} - (1+v)\left(1+\left(\frac{\alpha}{z}\right)^2\right)^{-0.5} + 0.5\left(1+\left(\frac{\alpha}{z}\right)^2\right)^{-1.5}\right] \tag{10}$$

where, Young's modulus of elasticity, E is 50 x 10^6 N/m^2, Poisson's ratio, ν is 0.25 for all three layers. The load of the vehicle is applied as stationary distributed pressure acting on a rectangular area of 0.46m x 0.3m symmetrical about x-z around surface point P of pavement Fig. 2. The result of the numerical model is compared to that of theoretical value determined by using Eqs. (8)-(10) (Boussinesq 1885) where α is the radius of a circle having the same area of the rectangle. The discrepancy of the result between the numerical model and that of theoretical value is about 1-4 % as shown in Table 5. Understandably, the error in displacement is relatively lower to that of stresses, since, displacement is the primary result quantity obtained directly solving equilibrium equation. Stresses, on the other hand, are derived result quantities determined by using primary quantity resulting in some finite element errors. The normal stresses about x and z are slightly different possibly due to unsymmetrical rectangle loading on the surface.

Table 5 Response of uniform half-space pavement at y = -1.0 m due to vertically distributed pressure acting on a rectangular area of 0.46m x 0.15m on the surface of the pavement

Parameter	Analytical	Numerical	Error (%)
u_y (m)	-1.939E-05	-1.90E-05	2.19
σ_y (N/m^2)	-36284.925	-35228	2.91
σ_x (N/m^2)	1477.097	1456.9	1.36
σ_z (N/m^2)	1477.097	1537.8	-4.11

Note: Here, negative sign represents compressive stress and downward deflection in model's sign convention

Table 6 Natural frequency of pavement

Mode	1	2	3	4	5
Frequency (rad/sec)	1.590	2.327	3.235	4.415	4.576

3.2 Damping in pavement

The modal analysis of pavement is carried out to determine the natural frequencies and estimate the damping characteristics of the pavement for dynamic analysis. Table 6 lists the natural frequencies of the pavement for the first five modes.

For the computation of damping matrix [C], Rayleigh damping damping is assumed for the pavement such that

$$[C] = \alpha_d[M] + \beta_d[K] \tag{11}$$

where α_d and β_d are the mass and stiffness damping coefficients. Assuming modal damping ratio corresponding to the natural frequency ω_i and ω_j of mode i and j of the pavement to be equal i.e $\xi_i = \xi_j = \xi$, the mass and stiffness damping coefficient can be determined using Eqs. (12) and (13) (Bathe 2005).

$$\alpha_d = \frac{2\omega_i\omega_j}{\omega_i + \omega_j} \tag{12}$$

$$\beta_d = \frac{2\xi}{\omega_i + \omega_j} \tag{13}$$

For the computation of the mass and stiffness damping coefficient, the damping ratio is required which depend on the frequency of the structure. The damping ratio is assumed to be constant in critical frequency range for simplicity, thus the damping coefficients have same critical damping ratio in the desired frequency range of the analysis. The pavement structure first natural frequency and loading dominant frequency is taken as frequency range for the determination of the damping ratio, which is assumed constant in that range. The mass and stiffness coefficient of Rayleigh damping is determined to be 0.1558 and 0.0145 using Eqs. (12)-(13) where, ω_i and ω_j are frequency for the constant Rayleigh damping in that range for which average of first three natural mode frequency and last two among the first five natural mode frequencies is considered. Experimentally, the damping ratio (ξ) of the pavement is found to be in the range of 2-5 % (Al-Qadi *et al*. 2008, Zhong *et al*. 2002). In this study, the damping ratio (ξ) is taken to be 5% in all layers.

3.3 Effect of different distribution of load on the pavement

A case-study is conducted to investigate effect of variable distribution of load on the pavement. For this purpose, the vehicular load on the pavement is modeled in three different ways: i) series of distributed pressure (Case I) ii) series of concentrated forces (Case II), and iii) a point concentrated force (Case III) each having same resultant force of 250 kN. The response of the pavement under these different spatial vehicle load cases moving with 10 m/sec is shown in Table 7. It can be

Table 7 Effect of different distribution of load on response of pavement

Case	y (m)	u_y (mm)	σ_y (kPa)	σ_x (kPa)	σ_z (kPa)
I	A (y=0.19m)	-0.9424	-109.40	-64.86	-3.21
	B (y=0.67m)	-0.8269	-23.18	-5.79	-0.27
II	A (y=0.19m)	-1.029	-236.3	-87.81	-4.634
	B(y=0.67m)	-0.893	-24.99	-6.943	-0.4302
III	A (y=0.19m)	-1.336	-471.2	-99	-5.394
	B (y=0.67m)	-1.019	-40.99	-7.99	-0.4587

Table 8 Peak response values of pavement under vehicle load moving with different speeds for elastic material

v (m/sec)	y (m)	u_y (mm)	σ_y (kPa)	σ_z (kPa)	ε_y (x 10^{-6})	ε_z (x 10^{-6})
10	A (y=0.19m)	-0.9424	-109.40	79.07	-238.80	91.90
	B (y=0.67m)	-0.8269	-23.18	10.41	-264.90	120.80
15	A (y=0.19m)	-0.9266	-99.30	73.41	-216.00	88.54
	B (y=0.67m)	-0.8195	-23.00	10.36	-262.30	120.60
20	A (y=0.19m)	-0.8925	-91.47	68.22	-198.10	85.07
	B (y=0.67m)	-0.7956	-22.83	10.27	-259.90	119.80
30	A (y=0.19m)	-0.8589	-82.54	61.38	-175.60	79.60
	B (y=0.67m)	-0.7583	-22.52	10.25	-257.30	118.60

observed from Table 7, the response of the pavement under the concentrated load is higher than under series of distributed pressure loads and concentrated load. For detailed response analysis, concentrated load is used for simplicity of modeling without much effect on the result of the analysis.

3.4 Linear response analysis

Another set of case study was done to evaluate the response of pavement under vehicular load moving with different velocities. A set of 4 different vehicular velocities of 10, 15, 20 and 30 m/sec are selected. The maximum responses for the cases taken are presented in Table 8. In general, the peak responses (displacement, stress and strain) of pavement under moving vehicle load is higher for lower velocity cases over the ones at higher velocities. The following sections give detail discussion on changes to each parameter to response analysis.

3.4.1 Vertical displacement (u_y) of pavement

The time history of vertical displacement at critical point A and B is shown in Fig. 7. The displacement of pavement is in direction of pressure and with the increase in depth, the displacement decreases. The two peaks observed on the curve during vehicle motion is due to tandem wheel configuration of vehicle. Each peak in time history curve occurs when the vehicle wheel is at or just after passing the critical point. For obvious reasons, the increase in vehicle speed resulted in earlier appearance of peak displacement in the pavement. However, with the

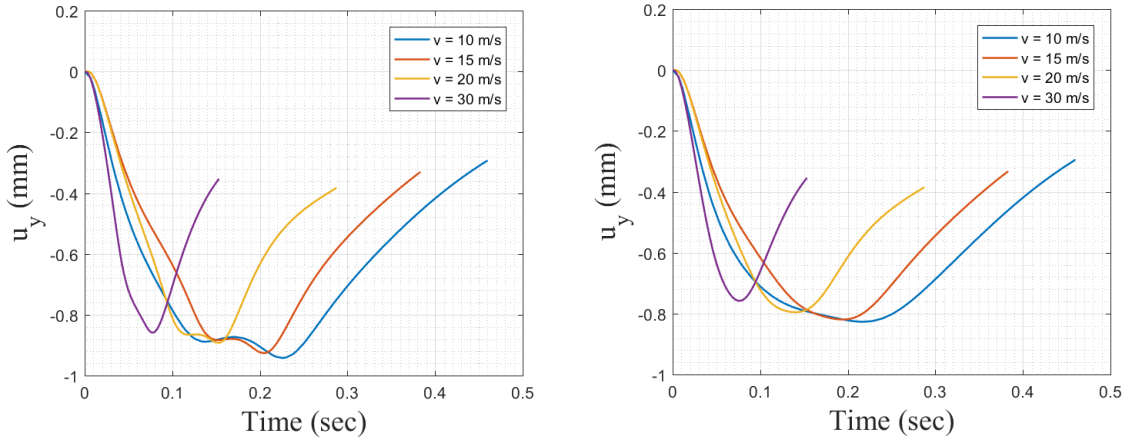

(a) at the bottom of asphalt layer (Point A) (b) at the top of subgrade layer (Point B)

Fig. 7 Vertical displacement time history under the moving vehicular loading

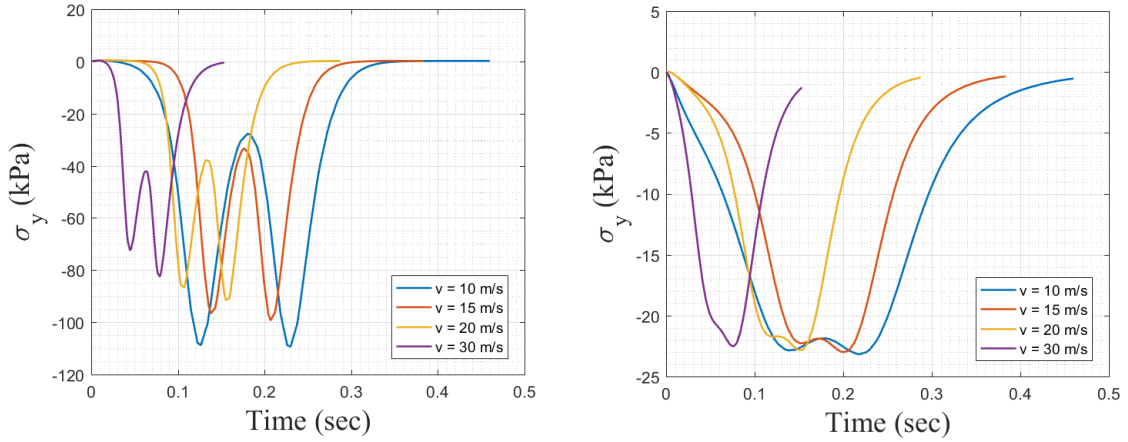

(a) at the bottom of asphalt layer (Point A) (b) at the top of subgrade layer (Point B)

Fig. 8 Vertical stress (σ_y) time history under the moving vehicular loading

increase in the vehicle speed, the magnitude of peak displacement decreases. As a representative example, there is an 8.8% decrement in vertical displacement (u_y) for moving load with speed of 10 m/sec compared to 30 m/sec speed at the bottom of asphalt and an 8.3% decrement at the top of subgrade for the same. This is understandably due to the reduction of contact time of vehicle and pavement with the increment in speed of vehicle. It should be noted that the presented results are in contrary to the one reported by Beskou *et al*. (2016b) and are better representative of the pavement response with variable speed. The effects of acceleration and deceleration, however, have not been considered during the current analysis and will be reported in authors' future works.

3.4.2 Stresses on pavement

The time history curves for vertical stresses (σ_y) are presented in Fig. 8. Fig. 8(a) shows time history for σ_y at point A, 190 mm from the top face and Fig. 8(b) at point B, 670 mm from the top

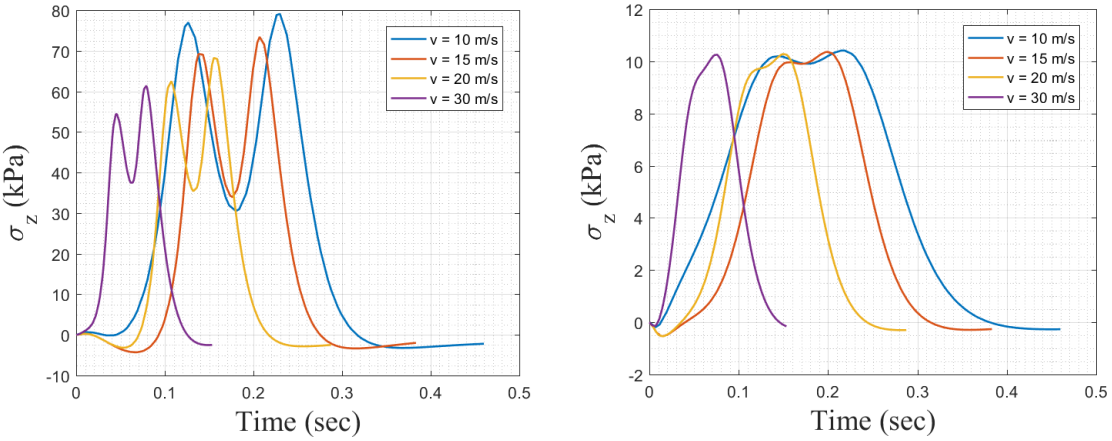

(a) at the bottom of asphalt layer (Point A) (b) at the top of subgrade layer (Point B)

Fig. 9 Lateral stress (σ_z) time history under the moving vehicular loading

face. There is in average 76 % decrease in vertical stress from point A to point B. Further, Table 8 shows that with the increase in the velocity, the magnitude of vertical stresses in the pavement layers goes on decreasing. The rate of decrease is more significant at the upper layers of the pavement and the effect is negligible at higher depths. As shown in Fig. 8 and Table 8, the reduction in magnitude of vertical stress at point A is 16 % for speeds of 20 m/sec and 10 m/sec and the same at point B was only 1.5 %. It can be observed that the two peaks also occur on the stresses time history. The vertical stress (σ_y) at base-asphalt and subgrade–base interface is always on compression during entire motion of the vehicle as shown in Fig. 8. Further, the stress variation is cyclic in nature and the cycle of variation in stress occur faster with increase in velocity of vehicle. The cyclic nature of stress goes on vanishing with increase in depth of the pavement. The lateral stresses along z-axis is both in tension and compression near the surface at point A as shown in Fig. 9. However, with the increase in the depth nature of lateral stresses predominantly becomes tension as illustrated in Fig. 9.

3.4.3 Strains on pavement

The time history curves for vertical strain (ε_y) are presented in Fig. 10. Fig. 10(a) shows time history for (ε_y) at point A 190 mm from the top face and Fig. 10(b) at point B 670 mm from the top face. There is in average 28 % increase in vertical strain from point A to point B. Although vertical stress decrease along depth, decrease in the modulus of elasticity along layer have higher impact in this case. Table 8 shows that with the increase in the velocity the magnitude of vertical strain in the pavement layers goes on decreasing. The rate of decrease is more significant at the upper layers of the pavement and the effect is negligible at higher depths. As shown in Fig. 10 and Table 8, the reduction in magnitude of vertical strain at point A is 26 % for speeds of 30 m/sec and 10 m/sec and the same at point B show 3% decrement. Here also, it can be observed that the two peaks also occur on the strain time history due to tandem wheel configuration. The vertical strain (ε_y) on base-asphalt and subgrade–base interface is always on compression during entire motion of the vehicle as shown in Fig. 10.

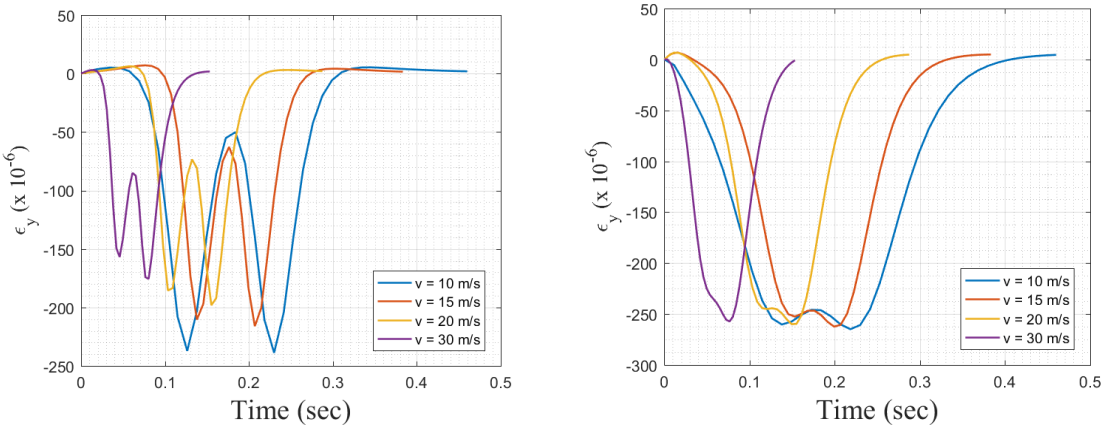

(a) at the bottom of asphalt layer (Point A) (b) at the top of subgrade layer (Point B)

Fig. 10 Vertical strain (ε_y) time history at under the moving vehicular loading

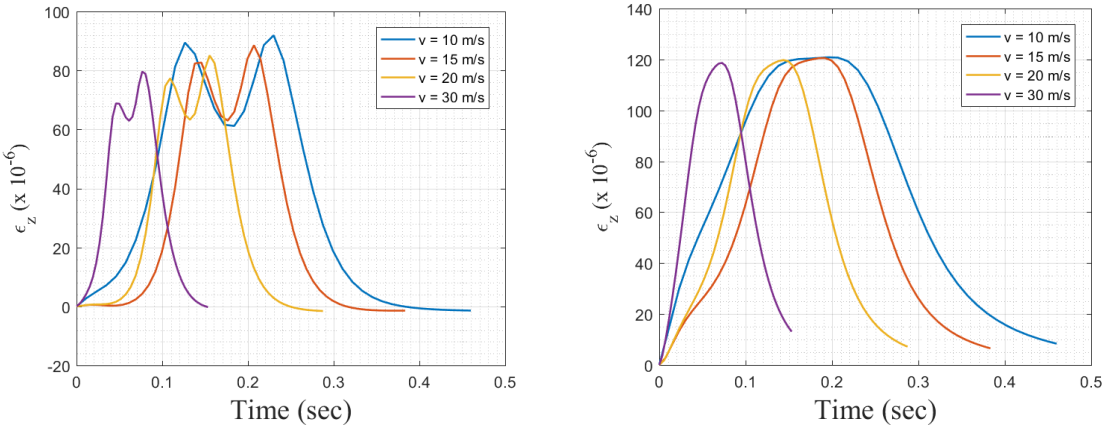

(a) at the bottom of asphalt layer (Point A) (b) at the top of subgrade layer (Point B)

Fig. 11 Lateral strain (ε_z) time history at under the moving vehicular loading

As in the stress, strain variation is also cyclic in nature and the cycle of variation in strain occur faster with increase in velocity of vehicle. The cyclic nature of strain goes on vanishing with increase in depth of the pavement. The lateral strain along z-axis is in tension along depth as shown in Fig. 11. There is in average of 39 % increase in strain ε_z respectively from point A to point B as in vertical strain. Further, Table 8 shows that with the increase in the velocity, the magnitude of tensile strains in the pavement layers goes on decreasing. Here again, the rate of decrease is more significant at the upper layers of the pavement and the effect is negligible at higher depths.

3.5 Non-linear response analysis

Similar to the linear case, a set of 4 different vehicular velocities of 10, 15, 20 and 30 m/sec are selected. The maximum responses for the cases taken are presented in Table 9. The response

Table 9 Peak response values of pavement under vehicle load moving with different speeds for nonlinear response analysis

v	y	uy	σy	σz	εy	εz
(m/s)	(m)	(mm)	(kPa)	(kPa)	(x 10-6)	(x 10-6)
10	A (y=0.19m)	-0.9849	-145.10	164.75	-132.1	77.10
	B (y=0.67m)	-0.8934	-21.60	0.98	-336.5	123.60
15	A (y=0.19m)	-0.9573	-130.50	151.15	-116.3	74.94
	B (y=0.67m)	-0.8506	-21.51	0.90	-333.8	122.40
20	A (y=0.19m)	-0.9048	-119.1	142.41	-104.4	73.01
	B (y=0.67m)	-0.8042	-21.37	0.88	-331.1	121.50
25	A (y=0.19m)	-0.8848	-106.20	128.97	-88.77	68.34
	B (y=0.67m)	-0.7896	-20.99	0.82	-324.9	118.90

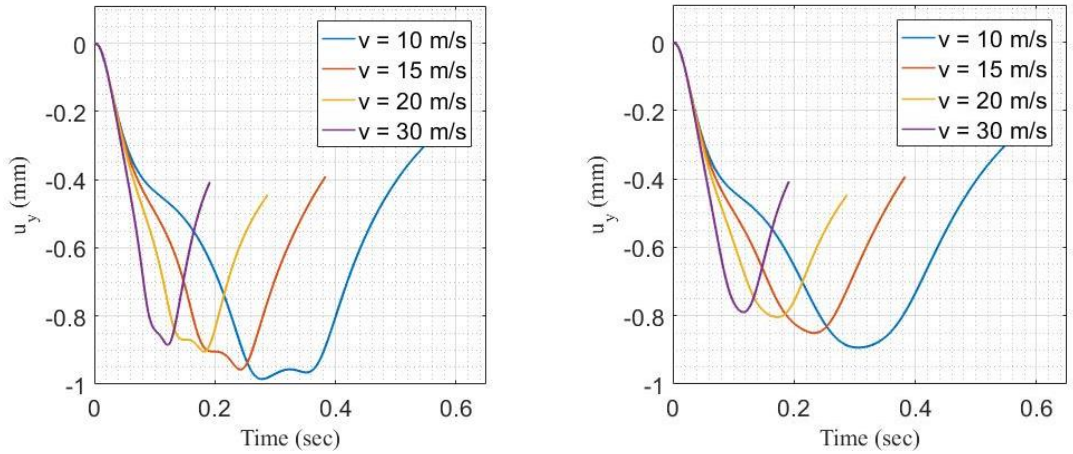

(a) at the bottom of asphalt layer (Point A) (b) at the top of subgrade layer (Point B)

Fig. 12 Vertical displacement time history under the moving vehicular loading

(displacement, stress and strain) of pavement having viscoelastic asphalt layer is higher than linear response of pavement. As a representative example, there is a 3.05% increment in vertical displacement (u_y) and 30.7% increment in vertical stress (σ_y) for non-linear pavement response compare to that of linear response at the bottom of asphalt layer. The magnitude of response of pavement decrease with increase of the vehicular speed as the result in linear pavement response. Furthermore, there is 7% decrease in vertical displacement and 17% decrease in vertical stress when constant velocity of vehicle increases from 15 m/s to 30 m/s.

3.5.1 Vertical displacement (u_y) of pavement

The time history of vertical displacement at critical point A and B is shown in Fig. 12. The displacement of pavement is in direction of pressure and with the increase in depth, the displacement decreases. The two peaks observed on the curve during vehicle motion is due to tandem wheel configuration of vehicle. Each peak in time history curve occurs when the vehicle

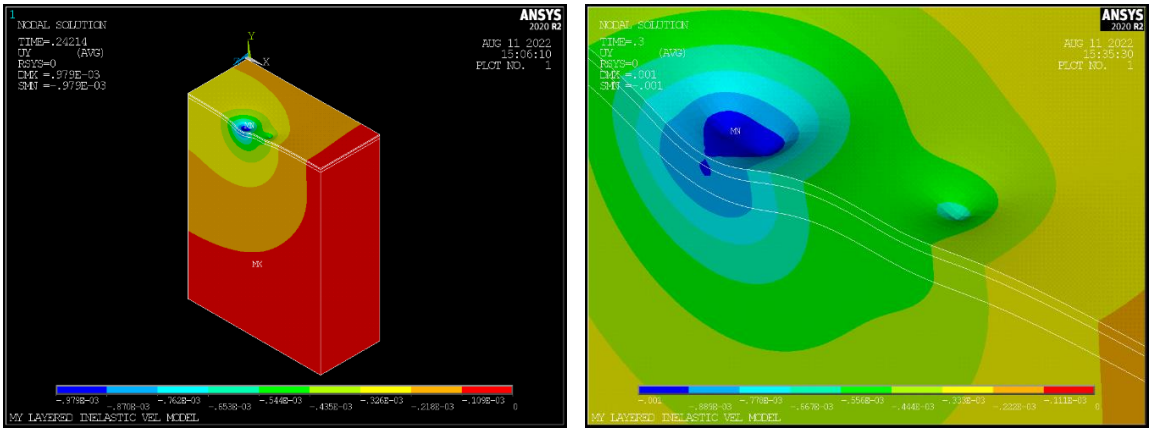

(a) Full view of model (b) Zoomed in view of model

Fig. 13 Vertical displacement contour under the vehicular loading at time T = 0.242 sec moving at constant velocity of 15 m/s

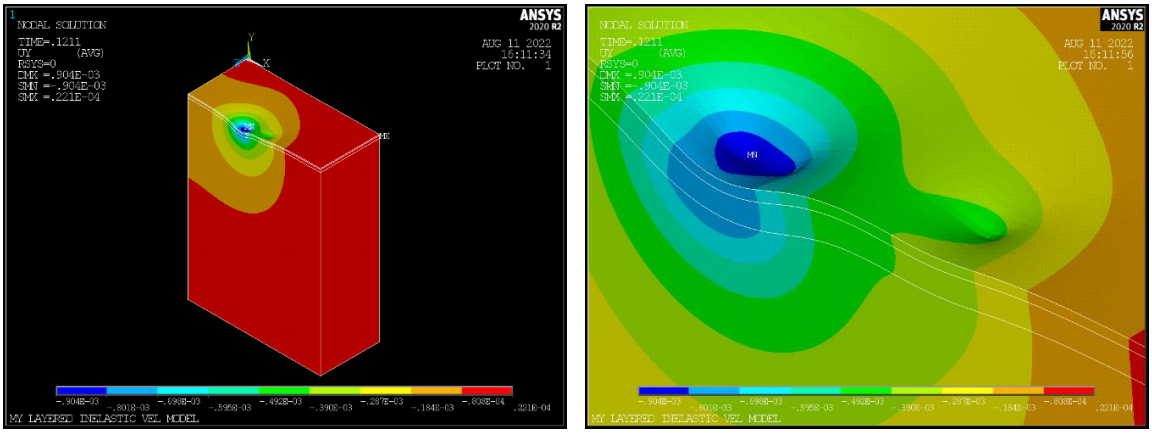

(a) Full view of model (b) Zoom in view of model

Fig. 14 Vertical displacement contour under the vehicular loading at time T = 0.121 sec moving at constant velocity of 30 m/s

wheel is at or just after passing the critical point. With the increase in the vehicle speed, the magnitude of displacement decreases. Similar observations were made for the linear response analysis as well, where there was reduction of contact time of vehicle and pavement with the increment in speed of vehicle. The effects of acceleration and deceleration, however, have not been considered during the current analysis and will be reported in authors' future works. Figs. 13 and 14 show the vertical displacement contours experienced by the pavement layers for velocity of 15 m/sec and 30 m/sec. Comparatively, higher deformation contour levels are seen for velocity of 15 m/sec with higher deformation at the rear tandem axle.

It should be noted that an average increment in vertical displacement of 3.05% at the bottom of asphalt layer (Point A) and 4.26% at the top of subgrade layer (Point B) was observed in nonlinear response analysis as compared to the linear analysis reported earlier.

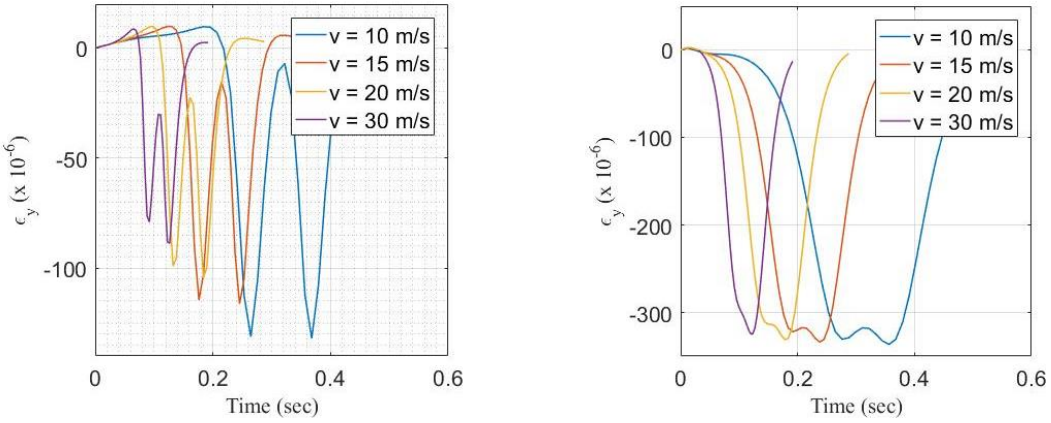

(a) at the bottom of asphalt layer (Point A) (b) at the top of subgrade layer (Point B)

Fig. 15 Vertical strain (ε_y) time history at under the moving vehicular loading

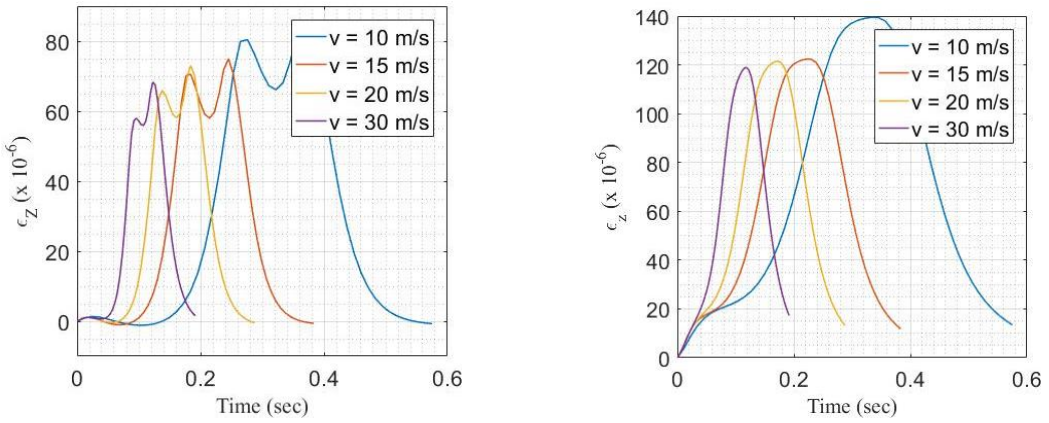

(a) at the bottom of asphalt layer (Point A) (b) at the top of subgrade layer (Point B)

Fig. 16 Lateral strain (ε_z) time history at under the moving vehicular loading

3.5.2 Strains on pavement

The time history curves for vertical strain (ε_y) are presented in Fig. 15. There is in average 217% increase in vertical strain from point A (asphalt – base interaction) to point B (base-subgrade interaction) although vertical stress decrease along depth. The increase in vertical strain is significant for nonlinear case as compared to the linear response analysis. Table 9 shows that with the increase in the velocity the magnitude of vertical strain in the pavement layers goes on decreasing. The rate of decrease is more significant at the upper layers of the pavement and the effect is negligible at higher depths. Similar to earlier findings, it can be observed that the two peaks also occur in the strain time history due to tandem wheel configuration. The vertical strain (ε_y) on base-asphalt and subgrade–base interface is always on compression during entire motion of the vehicle as shown in Fig. 15. Strain variation is also cyclic in nature and the cycle of variation occur faster with increase in velocity of vehicle. The cyclic nature of strain goes on vanishing with increase in depth of the pavement.

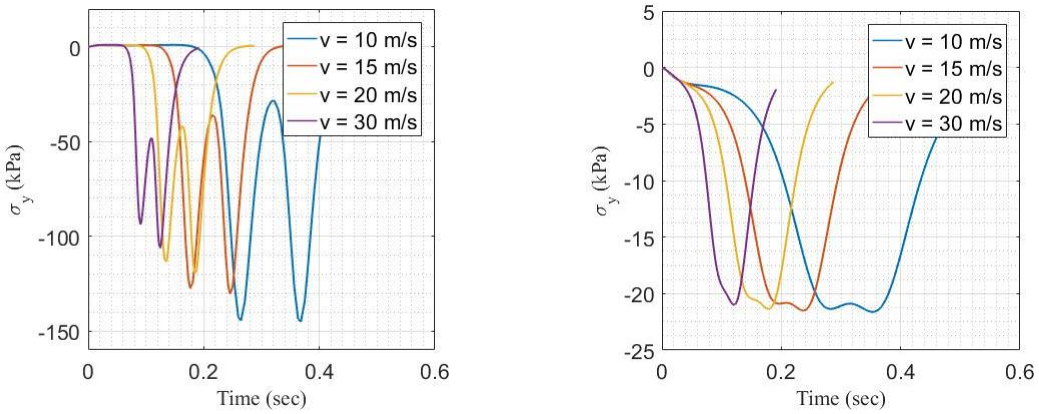

(a) at the bottom of asphalt layer (Point A) (b) at the top of subgrade layer (Point B)

Fig. 17 Vertical stress (σ_y) time history under the moving vehicular loading

The lateral strain along z-axis is in tension along depth as shown in Fig. 16. There is in average of 66 % increase in strain ε_z respectively from point A to point B as in vertical strain. Further, Table 9 shows that with the increase in the velocity the magnitude of tensile strains in the pavement layers goes on decreasing. The rate of decrease is more significant at the upper layers of the pavement and the effect is negligible at higher depths. The reduction in magnitude of strain (ε_z) at point A is 10 %, for speeds of 30 m/s and 10 m/s and 2 % at point B shown in Fig. 16.

3.5.3 Stresses on pavement

The time history curves for vertical stresses (σ_y) are presented in Fig. 17(a) at point A, 190 mm from the top face (asphalt – base interaction) and Fig. 17(b) at point B, 670 mm from the top face (base- subgrade interaction). There is in average 82 % decrease in vertical stress from point A to point B. Table 9 shows that with the increase in the velocity, the magnitude of vertical stresses in the pavement layers goes on decreasing. The rate of decrease is more significant at the upper layers of the pavement and the effect is negligible at higher depths. The reduction in magnitude of vertical stress at point A is 17 % for speeds of 15 m/s and 30 m/s and the same at point B was only 2 %. The vertical stress (σ_y) on base-asphalt and subgrade–base interface is always on compression during entire motion of the vehicle as shown in Fig. 17. The cycle of variation in stress occur faster with increase in velocity of vehicle and is more prominent at the bottom of asphalt layer. The cyclic nature of stress goes on vanishing with increase in depth of the pavement. Figs. 18 and 19 show the vertical stress contours experienced by the pavement layers for velocity of 15 m/sec and 30 m/sec.

The nonlinear results, when compared with the linear response analysis, show some interesting observations for the stress response quantity. There was a significant increment in vertical stress with an average value of 30.7% for nonlinear response analysis compared to the linear analysis at the bottom of asphalt layer (Point A). The same observation does not hold true at the top of subgrade layer (Point B), where, in contrary, there is slight decrement in the vertical stresses for nonlinear response analysis over the linear counterpart.

It should be noted that the response results, with higher displacements and stress components at lower vehicle velocity, are in contrary to previous notable literature (Beskou *et al*. 2016a, b) but

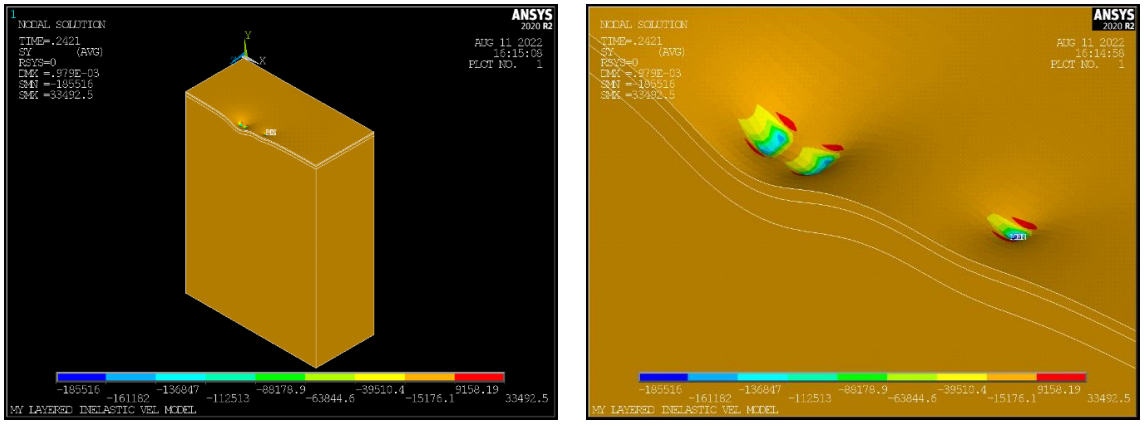

(a) Full view of model (b) Zoomed in view of model

Fig. 18 Vertical stress contour under the vehicular loading.at time T = 0.242 sec moving at constant velocity of 15 m/s

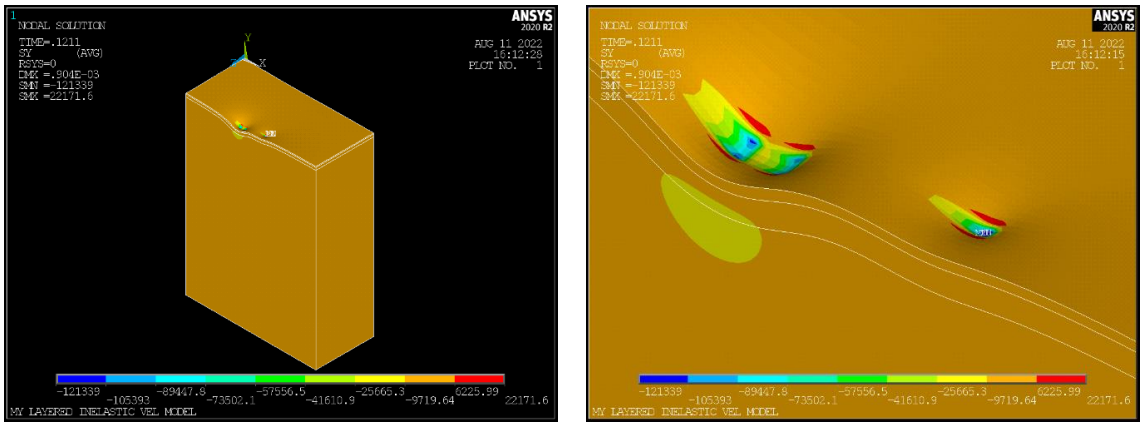

(a) Full view of model (b) Zoom in view of model

Fig. 19 Vertical stress contour under the vehicular loading.at time T = 0.121 sec moving at constant velocity of 30 m/s

are better representative of real scenario. The results presented and the discussions made reinforce the fact that higher level of pavement damage can be expected for the stretch of road where there is possibility of low speed traffic of relatively heavy vehicles.

4. Conclusions

The three-dimensional linear dynamic analysis of pavement is carried out considering material properties for a typical flexible pavement in Nepal using finite element software, ANSYS. The validated FE model is utilized to further analyze the response of pavement for various loading patterns of wheel load and variable vehicular speeds. The results show that, with the increase in speed of the vehicle, the response of the elastic as well as visco-elastic flexible pavement goes on

decreasing due the decrease in the contact time between tire and pavement at higher speeds. Further, the rate of decrease is more significant at the upper layers of the pavement and the effect is negligible at higher depths. As a representative example, decrements of 8.8% in peak vertical displacement and 24.5% in peak vertical stress were observed when the speed increased from 10 m/sec to 30 m/sec.

The responses measured in terms of displacement, stress and strain of pavement having viscoelastic asphalt layer is higher than its linear counterpart. There was a 3% increment in vertical displacement (u_y) and 24% increment in vertical stress (σ_y) for non-linear pavement response compared to that of linear response at the bottom of asphalt layer.

The authors plan to extend the results from the present work in future through further exploration involving experimentations and numerical methods to develop mechanistic-empirical design method as proposed by researchers (Beskou *et al*. 2016a, Khan *et al*. 2013, Sebaaly and Mamlouk 1988) and further investigate the fatigue and rutting life of pavements in Nepal.

Acknowledgments

This research is funded by Roads Board Nepal (RBN) under Nepal Government. The authors acknowledge the support provided by Center for Infrastructure Development Studies (CIDS), Institute of Engineering, Tribhuvan University. The authors would also like to thank Er. Pramod Tiwari, Er. Sangita Acharya and Er. Prabin Wagle for providing invaluable support during this study.

References

AASHTO (1993), "AASHTO Guide for Design of pavement structures", *International Conference on Sustainable Waste Management and Recycling: Construction Demolition Waste*.

Al-Qadi, I.L., Wang, H., Yoo, P.J. and Dessouky, S.H. (2008), "Dynamic analysis and in situ validation of perpetual pavement response to vehicular loading", *Transp. Res. Record*, **2087**, 29-39. https://doi.org/10.3141/2087-04.

Ali, B., Sadek, M. and Shahrour, I. (2009), "Finite-Element model for urban pavement rutting: Analysis of pavement rehabilitation methods", *J. Transp. Eng.*, **135**(4), 235-239. https://doi.org/10.1061/(ASCE)0733-947X(2009)135:4(235).

ANSYS (2013), *ANSYS Mechanical APDL Verification Manual*, ANSYS Inc. Southpointe, Canonsburg, PA.

Assogba, O.C., Tan, Y., Zhou, X., Zhang, C. and Anato, J.N. (2020), "Numerical investigation of the mechanical response of semi-rigid base asphalt pavement under traffic load and nonlinear temperature gradient effect", *Constr. Build. Mater.*, **235**, 117406. https://doi.org/10.1016/j.conbuildmat.2019.117406.

Bathe K.J. (2005), *Finite Element Procedures [M]*, in *Englewood Cliffs New Jersey*.

Berthelot, C.F., Allen, D.H. and Searcy, C.R. (2003), "Method for performing accelerated characterization of viscoelastic constitutive behavior of asphaltic concrete", *J. Mater. Civil Eng.*, **15**(5), 496-505. https://doi.org/10.1061/(asce)0899-1561(2003)15:5(496).

Beskou, N.D., Tsinopoulos, S.V. and Hatzigeorgiou, G.D. (2016), "Fatigue cracking failure criterion for flexible pavements under moving vehicles", *Soil Dyn. Earthq. Eng.*, **90**, 476-479. https://doi.org/10.1016/j.soildyn.2016.09.019.

Beskou, N.D., Tsinopoulos, S.V. and Theodorakopoulos, D.D. (2016), "Dynamic elastic analysis of 3-D flexible pavements under moving vehicles: A unified FEM treatment", *Soil Dyn. Earthq. Eng.*, **82**, 63-72.

https://doi.org/10.1016/j.soildyn.2015.11.013.
Boussinesq, J. (1885), *Application Des Potentiels*, Gauthier-Villars Publications, Paris, France.
Byzyka, J., Rahman, M., Chamberlain, D.A. (2020), "Thermal analysis of hot mix asphalt pothole repair by finite-element method", *J. Transp. Eng. B Pavements*, **146**(3), 04020029. https://doi.org/10.1061/jpeodx.0000156.
Cebon, D. (1999), *Handbook of Vehicle-Road Interaction*, Taylor & Francis, London, U.K.
Cho, Y.H., McCullough, B.F. and Weissmann, J. (1996), "Considerations on finite-element method application in pavement structural analysis", *Transp. Res. Record*, **1539**(1), 96-101. https://doi.org/10.1177/0361198196153900113.
De Beer, M. (1996), "Measurement of tyre pavement interface stresses under moving wheel loads", *Heavy Vehicle Syst.*, **3**(1-2), 97-115. https://doi.org/10.1504/IJHVS.1996.054553
DeSalva, Gabriel J., Swanson, J.A. (1985a), *ANSYS Engineering Analysis System User'S Manual*, Pa. :Swanson Analysis Systems, Houston, U.S.A.
DeSalva, Gabriel J., Swanson, J.A. (1985b), "*ANSYS Mechanical APDL Basic Design Guide*, Pa. :Swanson Analysis Systems, Houston, U.S.A.
DOR (2021), *Guidelines for the Design of Flexible Pavements 2014 (Second Edition)*, Department of Roads; Lalitpur, Nepal.
González, J.M., Miquel Canet, J., Oller, S. and Miró, R. (2007), "A viscoplastic constitutive model with strain rate variables for asphalt mixtures-numerical simulation", *Comput. Mater. Sci.*, **38**(4), 543-560. https://doi.org/10.1016/j.commatsci.2006.03.013.
Gungor, O.E., Al-Qadi, I.L., Gamez, A. and Hernandez, J.A. (2016), *In-situ validation of three-dimensional pavement finite element models*, in *The Roles of Accelerated Pavement Testing in Pavement Sustainability: Engineering, Environment, and Economics*, Springer International Publishing. https://doi.org/10.1007/978-3-319-42797-3_10.
Hatzigeorgiou George D., G.D. and Beskos, D.E. (2010), "Soil-structure interaction effects on seismic inelastic analysis of 3-D tunnels", *Soil Dyn. Earthq. Eng.*, **30**(9), 851-861. https://doi.org/10.1016/j.soildyn.2010.03.010.
Howard, I.L. and Warren, K.A. (2009), "Finite-element modeling of instrumented flexible pavements under stationary transient loading", *J. Transp. Eng.*, **135**(2), 53-61. https://doi.org/10.1061/(ASCE)0733-947X(2009)135:2(53).
Huang, B., Mohammad, L.N. and Rasoulian, M. (2001), "Three-dimensional numerical simulation of asphalt pavement at Louisiana accelerated loading facility", *Transp. Res. Record*, **1764**(1764), 44-58. https://doi.org/10.3141/1764-06.
Huang, C.W., Abu Al-Rub, R.K., Masad, E.A. and Little, D.N. (2011), "Three-dimensional simulations of asphalt pavement permanent deformation using a nonlinear viscoelastic and viscoplastic model", *J. Mater. Civil Eng.*, **23**(1), 56-68. https://doi.org/10.1061/(asce)mt.1943-5533.0000022.
Huang, Y.H. (2004), *Pavement Analysis and Design*, Prentic-Hall In Inc., New Jersey, USA.
IRC (2018), *Guidelines for the Design of Flexible Pavements*, Indian Roads Congress Fourth (Revision), New Delhi, India.
Khan, S., Nagabhushana, M.N., Tiwari, D. and Jain, P.K. (2013), "Rutting in flexible pavement: An approach of evaluation with accelerated pavement testing facility", *Procedia - Social and Behavioral Sciences*, **104**, 149-157. https://doi.org/10.1016/j.sbspro.2013.11.107.
Li, S., Guo, Z. and Yang, Y. (2015), "Dynamic viscoelastic response of an instrumented asphalt pavement under various axles with non-uniform stress distribution", *Road Mater. Pavement Des.*, **17**(2), 446-465. https://doi.org/10.1080/14680629.2015.1080178.
Li, M., Wang, H., Xu, G. and Xie, P. (2017), "Finite element modeling and parametric analysis of viscoelastic and nonlinear pavement responses under dynamic FWD loading", *Constr. Build. Mater.*, **141**, 23-35. https://doi.org/10.1016/j.conbuildmat.2017.02.096.
Lu, Y. and Wright, P.J. (1998), "Numerical approach of visco-elastoplastic analysis for asphalt mixtures", *Comput. Struct.*, **69**(2), 139-147. https://doi.org/10.1016/S0045-7949(98)00139-4.
Melaku, S., Qiu H. (2015), "Finite element analysis of pavement design using ANSYS finite element code",

Proceeding of the 2nd Int. Conf. on Civil Engineering, Energy and Environment, 64-69, Hubei, China.
Road Note 31 (1984), Road note 31: A guide to the structural design of bitumen surfaced roads in tropical and subtropical countries, Transport and Road Research Laboratory (TRRL); Berkshire, U.K.
Saleeb, A., Liang, R.Y., Qablan, H.A.L. and Powers, D. (2005), "Numerical simulation techniques for HMA rutting under loaded wheel tester", *Int. J. Pavement Eng.*, **6**(1), 57-66. https://doi.org/10.1080/10298430500068704.
Saint-Venant, B.D. (1855), "Mémoire sur la torsion des prismes. Mémoires des Savants étrangers", *Acad. Sci., Paris*, **14**, 223-560.
Sebaaly, P.E. and Mamlouk, M.S. (1988), "Development of dynamic fatigue failure criterion", *J. Transp. Eng.*, **114**(4), 450-464. https://doi.org/10.1061/(ASCE)0733-947X(1988)114:4(450).
Tata-Motor (2020), Vehicle type Truck LPK 2518 6S 20 cum, TATA Motors Limited, Mumbai, India. https://tatatrucks.tatamotors.com/tata-trucks/tippers/tata-lpk-2518/tata-lpk-2518-6s-20cum-specifications.aspx#specifications
Yoo, P.J. and Al-Qadi, I.L. (2007), "Effect of transient dynamic loading on flexible pavements", *Transp. Res. Record*, **1990**(1990), 129-140. https://doi.org/10.3141/1990-15
Zaghloul, S., White, T., Drnevich, V. and Coree, B. (1994), "Dynamic analysis of FWD loading and pavement response using a three-dimensional dynamic finite-element program", *ASTM Special Tech. Publication*, **1198**, 125-125.
Zhong, X.G., Zeng, X. and Rose, J.G. (2002), "Shear modulus and damping ratio of rubber-modified asphalt mixes and unsaturated subgrade soils", *J. Mater. Civil Eng.*, **14**(6), 496-502. https://doi.org/10.1061/(asce)0899-1561(2002)14:6(496).

TK